

Direct synthesis of single-crystal bilayer graphene on various dielectric substrates

Xiangping Chen^{1, #}, Xianqin Xing^{2, #}, Wenyu Liu², Zhanjie Lu², Hao Ying², Le Huang³, Zhiyong Zhang³, Shunqing Wu⁴, Zhihai Cheng² and Shanshan Chen^{2, *}

¹Tsinghua-Berkeley Shenzhen Institute (TBSI), Tsinghua University, Shenzhen 518055, China

²Department of Physics and Beijing Key Laboratory of Optoelectronic Functional Natural Materials & Micro-nano Devices, Renmin University of China, Beijing 100872, China

³Key Laboratory for the Physics and Chemistry of Nanodevices and Department of Electronics, Peking University, Beijing, 100871, China

⁴Collaborative Innovation Center for Optoelectronic Semiconductors and Efficient Devices, Department of Physics, Xiamen University, Xiamen 361005, China

X. Chen and X. Xing contributed equally to this work.

* Corresponding author: schen@ruc.edu.cn

Abstract

In this work, a novel method to grow high-quality and large bilayer graphene (BLG) directly on various dielectric substrates was demonstrated. Large area single-crystal monolayer graphene was applied as a seeding layer to facilitate the homo-epitaxial synthesis of single crystal BLG directly on insulating substrates. The Cu nano-powders (Cu NP) with nanostructure and high surface-area were used as the remote catalysis to provide long-lasting catalytic activity during the graphene growth. The TEM results confirms the single-crystalline nature of the BLG domains, which validates the superiority of the homo-epitaxial growth technique. The as-grown BLG show comparable quality with the CVD-grown BLG on metal surface. Field-effect transistors directly fabricated on the as-grown BLG/SiO₂/Si showed a room temperature carrier mobility as high as 2297 cm² V⁻¹ s⁻¹.

Keyword: Bernal-stacked bilayer graphene, remote catalysis, homo-epitaxial growth, dielectric substrates

1. Introduction

Bernal-stacked bilayer graphene (BLG) features appealing physical properties such as the possibility of opening and tuning an electronic bandgap¹⁻⁵ or engineering of quantum dots for a single-electron manipulation⁶, making it a candidate of interest for electronic and photonic device applications.⁷⁻⁹ While chemical vapor deposition (CVD) on metal substrates, such as Ni¹⁰⁻¹¹, Cu¹²⁻²⁴, and Cu-Ni alloys²⁵⁻²⁸, has been shown to be capable in producing large-scale BLG or multilayer graphene. Thus, developing an effective method to directly synthesize the large-area BLG on dielectric substrates is crucial for fundamental research and further industrial-scale fabrication.

Many techniques have been reported that the direct growth of graphene on various dielectric substrates, such as Si₃N₄²⁹⁻³¹, SrTiO₃³², SiO₂^{29, 31, 33-44}, Al₂O₃^{29, 31, 42, 45}, glass⁴⁶⁻⁴⁸ and h-BN^{31, 49-50}. For the gaseous carbon source, the approaches to grow the graphene on dielectric substrates can be sorted into four categories. The first is direct decomposing the carbon source and depositing on the dielectric substrates.^{29-30, 32, 41, 45} This approach always requires ultrahigh growth temperature and extremely long growth time, but the obtained graphene always suffers from lower crystalline quality, and smaller domain sizes. The second is applying the carbon diffusion mode that direct growth of graphene onto the interface between the metal films and dielectric substrates.^{38-39, 43} This approach can reduce the growth temperature and time, improve the graphene quality, however it is difficult to control the thickness and the domain size of graphene is always small. The third is using the plasma enhanced CVD to supply the carbon radical,^{36, 40, 50} which can further reduce the growth temperature to lower than

700 °C. However, the quality of PECVD grown graphene was not very high and island growth and vertical graphene sheets are typically observed. The fourth is using the metal vapor as the catalysis to promote the dehydrogenation of the carbon source to fabricate graphene on the dielectric substrates^{33, 35, 37, 51}. Most of these works typically yielded poly-crystalline films composed of graphene domains of less than 10 μm. Therefore, controllably synthesis of high quality BLG on dielectric substrates with minimal crystalline defects and maximal area of Bernal stacking are still challenging.

Triggering by the wafer-scale single crystal SLG synthesis on single crystal Ge (110) substrate,^{7, 26, 52-53} and homo-epitaxial growth graphene on the highly oriented pyrolytic graphite (HOPG)⁴⁰, we apply the large-area CVD-grown single-crystal SLG were applied as the single crystal substrate or seeding layers to induce the homo-epitaxial growth of single-crystal BLG. The copper nano-powders (Cu NP) was utilized as the remote catalyst to promote the methane decomposition and further to supply the active carbon species. Instead of using single crystal metal or dielectric substrate, the single-crystal SLG seeding layer was transferred onto the various dielectric substrates to lower the energy barrier for carbon diffusivity on the dielectric substrate surface for the subsequent homo-epitaxial growth of single-crystal BLG. Thereby, the BLG growth efficiency has been greatly enhanced, and 92% BLG coverage and single domain with the diagonal length up to ~70μm after 120 min growth are realized. Owing to almost all BLG domains are well aligned as the same orientation of the seeding SLG layer, this technique has the potential to obtained large-area single-crystal BLG, when the BLG domains coalesce into a uniform layer. Raman spectroscopy and transmission electron

microscopy (TEM) results confirmed that the as grown BLG are typically with Bernal stack order with superior quality. Field-effect transistors (FET) were directly fabricated on graphene/SiO₂/Si for evaluating their electric properties. FET measurements showed that the graphene bilayer had a single crystallographic orientation with carrier mobility as high as 2297 cm² V⁻¹ s⁻¹.

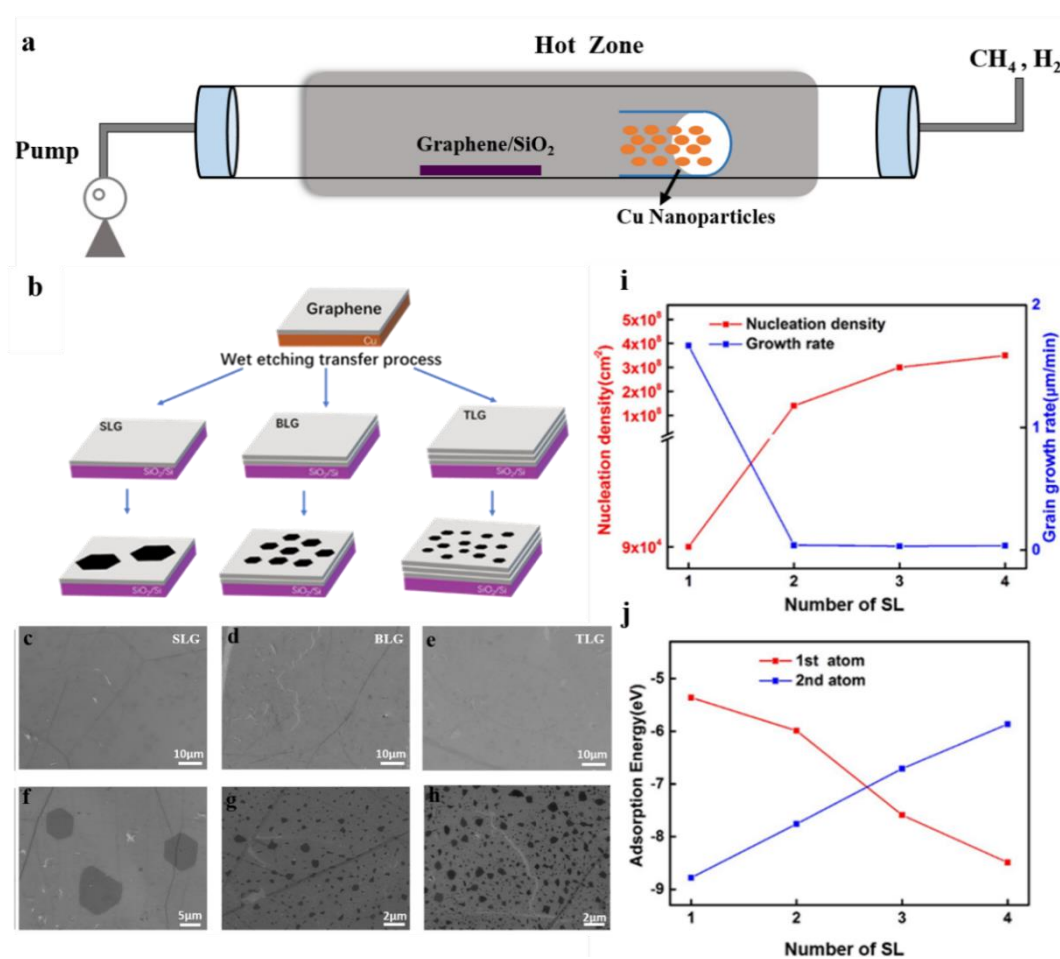


Figure 1. (a) Schematic diagram of Cu NP used as the floating catalyst in the CVD system. (b) Schematic diagram of epitaxial growth of graphene on graphene/dielectric substrates. (c-e) SEM images of SLG, BLG and TLG transferred onto a 300 nm SiO₂/Si substrate, respectively. (f-h) SEM images of epitaxial graphene grains grown on the corresponding substrates in (c-e), respectively. (i) Plots of nucleation density and graphene grain growth rate as a function of the number of graphene layers transferred onto the target substrates. (j) Plots of the adsorption energy of single carbon atom and the second carbon atom as a function of the number of graphene layers.

2. Experimental methods

2.1 Preparation of Single-Crystal SLG

Large area single crystal graphene grains were firstly grown on Cu (25 μm thick, Alfa Aesar, stock No.46365) foil which was electropolished using a home-built electrochemical cell and then made into the form of a Cu enclosure. For a typical growth process, the Cu enclosure was heated up to 1030 $^{\circ}\text{C}$ and annealed for 10 min under vacuum (2 mTorr), then graphene was grown in 1 sccm CH_4 and 50 sccm H_2 for 3 h (586 mTorr). After growth, the system was cooled down rapidly to room temperature in the same gaseous atmosphere. The graphene domains on the inner surface of Cu pocket were transferred onto various dielectric substrates (e.g. 300 nm SiO_2 /Si, sapphire and quartz) using a PMMA-assisted method.

2.2 Synthesis of Single-crystal BLG

The synthesis of single-crystal bilayer graphene domains on single-crystal monolayer graphene (SLG) was carried out in a low-pressure CVD system. Cu NP was used as the floating catalyst placed in the upper steam (Figure 1a). The insulating substrates with transferred SLG were then inserted to the center of quartz tube furnace and heated up to 1000 $^{\circ}\text{C}$ with 10 sccm H_2 (partial pressure of 120 mTorr) for 120 min to obtain a clean graphene seeding surface by further removing the residues caused by transfer. Various CH_4 flow of 5, 10, 15, and 20 sccm were introduced subsequently. After 1 h of exposure to CH_4 and H_2 , the samples were rapidly cooled down to room temperature.

2.3 Characterization

Scanning electron microscopy (SEM) images were obtained using a Zeiss Sigma

scanning electron microscope. Transmission electron microscopy (TEM) was performed with FEI TECNAI G F20 transmission electron microscope operated at 200 kV. Raman spectra were recorded at room temperature using a micro Raman spectrometer (Alpha 300, WiTec) with a 488 nm laser.

2.4 Device Fabrication and Electrical Measurements:

The electrical properties of the single-crystal bilayer graphene were characterized by fabricating dual-gate graphene FET devices directly on the as-grown graphene films on 300 nm SiO₂ /Si substrates. The device fabrication composed of four processes based on electron-beam lithography (EBL). First, the graphene channel was patterned (L/W = 9 μm/5 μm) and needless graphene was etched by oxygen plasma (Power = 100 W, 40 seconds). Second, a 3 nm thick yttrium strip was deposited cross the channel. After exposure in air at 240 °C for 30 min, Yttrium oxide (Y₂O₃) (5 nm) formed above the strip. Third, 20 nm Hafnium oxide (HfO₂) was grown by atomic layer deposition (ALD). The combination of Y₂O₃ and HfO₂ acted as reliable top gate dielectrics. Finally, the source/drain/gate electrodes (Ti/Au: 5/30 nm) were deposited by using e-beam evaporation. During the back-gate transfer measurements, the doped silicon substrate was utilized as the back gate. The FET characteristics were measured in air at room temperature. A Keithley 4200SC semiconductor parameter analyzer was used to measure the electrical characteristics of the devices.

3. Results and Discussion

The sub-centimeter single-crystal SLG was grown on Cu foil via low pressure CVD

process as reported previously^{5, 54}, and then the as-grown SLG films served as the SL were transferred onto the target substrates, e.g. 300nm SiO₂/Si, sapphire and quartz (Figure 1a). After 1h growth (See Experimental Section for more details), the bilayer and multilayer graphene domains with quasi-hexagonal structure were successfully formed on top of the SL, as shown in Figure 1f-h. It's noticed that the domain size and nucleation density of the as-grown graphene varies on the different thickness of the seeding layer. The corresponding statistics results plotted in Figure 1i showed that the nucleation density of as-grown graphene domains increased as the number of graphene seeding layers increased from one, two, three to four. However, the growth rate of the graphene domains dropped sharply as the number of graphene seeding layers added from one to two layers then plateaued out. To gain an insightful understanding on the evolution of the growth behavior, density functional theory (DFT) calculations were carried out (see Supporting Information for more details). As shown in Figure 1j, with the increasing number of graphene seeding layers, the absorption energy of the first C atom absorbed on graphene reduced quickly, whereas the absorption energy of the second C atom increases dramatically. The calculation results indicate that the enlarging of the ad-layer graphene domains needs more energy than forming the new nucleation when the thickness of the seeding layer increases, which explaining our experimental phenomenon accordingly. Furthermore, we noticed that there are no graphene nuclei formed on the bare SiO₂ surface in our experiments. When we prolong the growth time to 3 h, some micron-sized graphene flakes with poor quality were observed. Combined with the DFT calculations results, the crucial role of graphene

seeding layer to promote the homo-epitaxial growth of the ad-layer graphene.

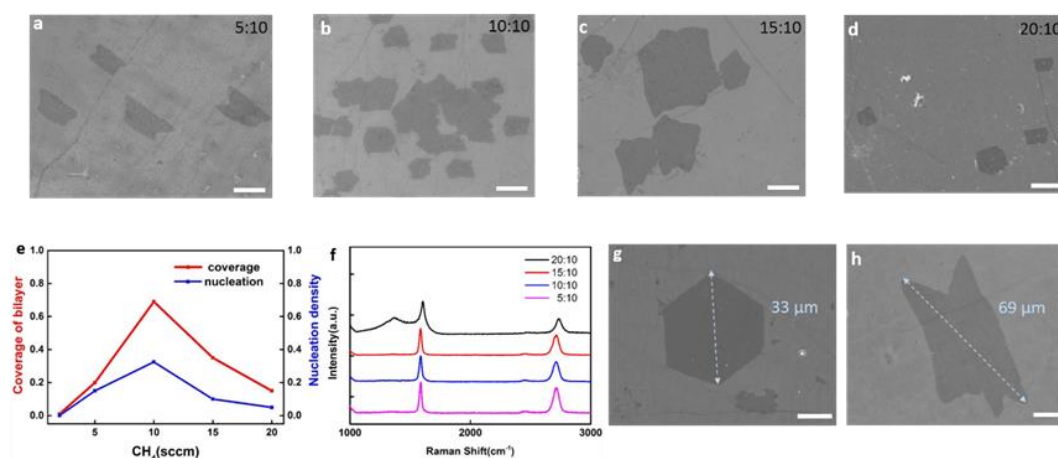


Figure 2. (a-d) SEM images of bilayer graphene synthesized on SLG/SiO₂/Si substrates under the same growth conditions with different CH₄/H₂ ratio for 5:10(a), 10:10(b), 15:10(c), and 20:10(d). (e) Plots of coverage and nucleation density of bilayer graphene as a function of CH₄ flow with constant H₂ flow (10sccm). (f) Typical Raman spectra of the samples grown at various CH₄ flow. (g-h) SEM images of single-crystal bilayer graphene domains with hexagonal and lobed structures, the largest domain size can be reached to 69µm. Scale bar: 10µm.

The key elements to direct synthesis of graphene through the Cu NP assisted graphene seeding growth method include the annealing time and CH₄ concentration. In contrast to the typical process for graphene growth, we annealed the substrates at 1000 °C in H₂ flow for 120 min to remove any organic residues caused by SLG transfer and to activate the growth sites. Typically, no growth would happen during the first 2 h even with CH₄ flow throughout the whole procedure. In addition, the effect of CH₄ concentration was studied by varying CH₄ flow while maintaining H₂ flow the same (10 sccm). Figure 2 a-d show the SEM images of BLG with different growth gas ratio (including CH₄:H₂ = 5:10, 10:10, 15:10, and 20:10). The coverage and nucleation density of the BLG both firstly increases then decreases with the increasing CH₄ flow, showing an inverted V shape as exhibited in Figure 2e. Some BLG domains even merges together to form the continuous film in Figure 2b. Figure 2f shows the Raman

spectra of the BLG under various reaction gas proportions. High quality BLG with invisible D peak were obtained for CH₄ flow no more than 20 sccm. When added the CH₄ flow up to 20sccm, the Raman spectrum shows a significant D peak and a border G peak, indicating a much lower crystalline quality⁵⁵⁻⁵⁶. As a consequence, the condition of CH₄:H₂ = 10:10 can be considered as the optimized condition to obtain BLG with higher nuclei density and larger coverage. Figure 2h shows some large BLG domains with the diagonal length up to 69 μm after 1h growth on SLG/SiO₂/Si wafer, which has been significantly improved than the ~ 11 μm monolayer graphene domain directly synthesized on SiO₂/Si wafer after 72 h⁵⁷. Besides, the Cu NPs assisted graphene seeding growth technique could be applied successfully on various dielectric substrates, for instance, quartz and sapphire (See Figure S2 in Supporting Information for more details).

Figure 3 c-d show the Raman maps of the G peak (1520 – 1640 cm⁻¹) and the full width of half maximum (FWHM) of 2D peak (2620 – 2780 cm⁻¹) from the region shown in Figure 3a, respectively. The relative dark region in Figure 3c corresponds to the SLG and the bright regions corresponds to the BLG. Together with the FWHM of 2D map in Figure 3d, it is clearly that large BLG domain exhibit Bernal stacking feature. Counts all of the BLG domains that obtained under the optimized growth condition, the AB-stacked bilayer graphene consists of ~ 96% of the total bilayer area (Figure 3e). Figure 3g and 3h show the I_{2D}/I_G ratio of the Raman spectra used to determine the AB stacking and the histograms of 2D band FWHM values. The I_{2D}/I_G ratio of the as-grown BLG is 0.95 ± 0.5 and the FWHM values of the 2D band are 48.0 ± 2 cm⁻¹. In comparison with

the 2D band FWHM values from the transferred AB-stacked BLG synthesized directly on Cu foil through grow from below technique¹³ (Figure 3i, FWHM = $53 \pm 2 \text{ cm}^{-1}$), and the sample mechanically stacked by two monolayer graphene films on the SiO₂/Si (Figure 3j, FWHM = $58 \pm 2 \text{ cm}^{-1}$), the bilayer graphene film growth on seeding layer displays a smaller FWHM which indicates an excellent quality^{20, 58}.

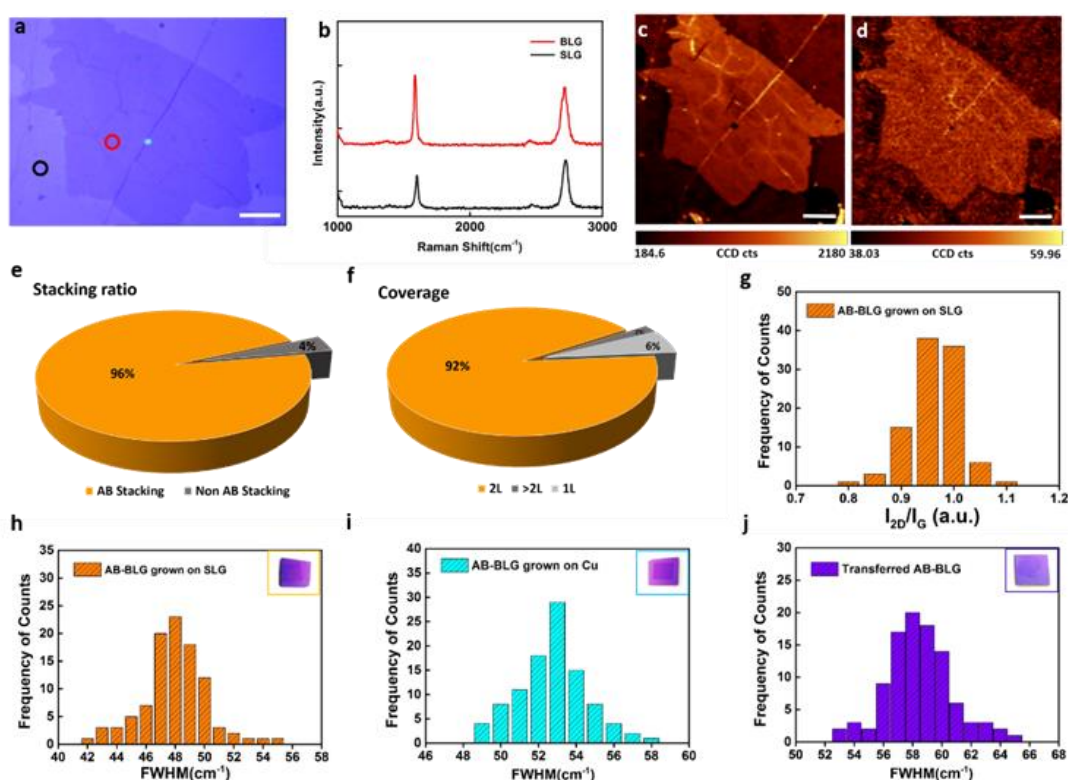


Figure 3. (a) Optical image of single-crystal BLG domain. (b) Raman spectra of the SLG and BLG areas from (a). (c-d) Raman map of G band intensity ($1520 - 1640 \text{ cm}^{-1}$) and 2D band FWHM ($2640 - 2780 \text{ cm}^{-1}$) of the same BLG grain in (a). (e-f) Stacking ratio and coverage statistics for the BLG sample grown based on optimized conditions. (g) Histogram of the I_{2D}/I_G ratio of the as-grown BLG. (h-j) Histograms of the Raman spectrum 2D band FWHM values of BLG grown through the single crystal SLG seeding technique (h), directly grown on Cu foil through grow from below technique (i), and by transferred additional monolayer graphene onto the SLG/SiO₂/Si substrate (j). The insets show the corresponding photographs of the samples on 300 nm SiO₂/Si wafer. Scale bar: 10 μm .

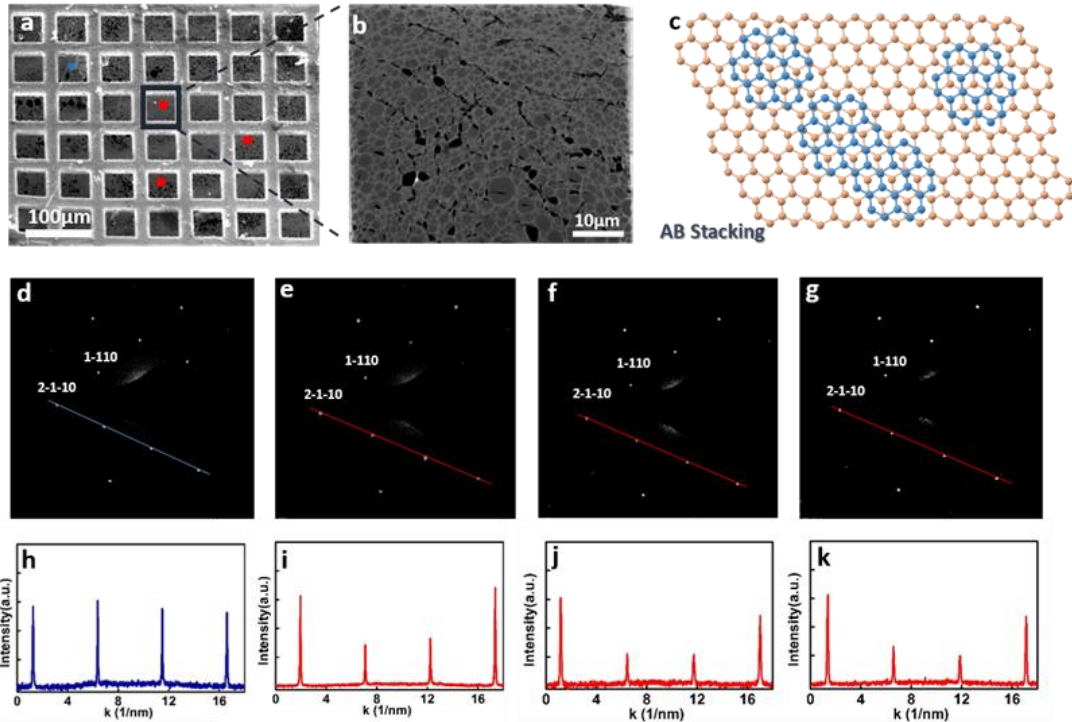


Figure 4. (a) SEM image of the as-grown BLG transferred onto the TEM grid. The blue and red circles denote the single crystal graphene substrate and BLG area, respectively. (b) Higher magnification SEM images of the corresponding black square marked in (a). (c) A schematic drawing of the synthesis of AB stacked bilayer graphene on the single crystal graphene seeding layer. (d) SAED pattern of the monolayer graphene in the blue circle region marked in (a). (e-f) SAED patterns of the as-grown BLG in the red circle regions marked in (a), all the three regions have the same orientation as the seeding layer. (h-k) Intensity profiles along the lines in (d-g), respectively.

The epitaxial growth nature was further evidenced by the crystalline structure of the as-grown BLG studied by transmission electron microscopy (TEM). The BLG film grown on large single crystal SLG seeding substrate was further transferred onto the TEM grid by etching away the SiO₂/Si substrate. A low magnification SEM image is displayed in Figure 4a, where the blue and red circles indicate SLG seeding area and as-grown BLG areas, respectively. Typical selected area electron diffraction (SAED) pattern of the seeding graphene in Figure 4a generate a single set of 6-fold symmetric diffraction spot (Figure 4d) with the diffraction intensity ratio of the outer (2-1-10) peak over the inner (1-110) peak is approximately 1 (Figure 4 h), indicating the single-

crystalline nature of the monolayer graphene seeding layer. Meanwhile, SAED patterns (Figure 4e-g) from the marked red regions in Figure 4a show the similar diffraction patterns as the seeding monolayer graphene, with the diffraction intensity ratio of the outer peak over the inner peak is approximately 2 (Figure 4i-k), which evidenced the AB stacking order of the as-grown bilayer film. The same crystalline orientation of the bilayer graphene confirms that the second layer graphene were epitaxial grown on the transferred single crystal monolayer graphene as expected^{12, 20, 58}. As schematically illustrated in Figure 4c, the initial multiple BLG nuclei occur with perfect rotational alignment on top of the single-crystalline graphene monolayer substrate, and these aligned nuclei can grow and coalesce into a uniform single-crystal layer without grain boundary defects, even if the nucleation density is high.

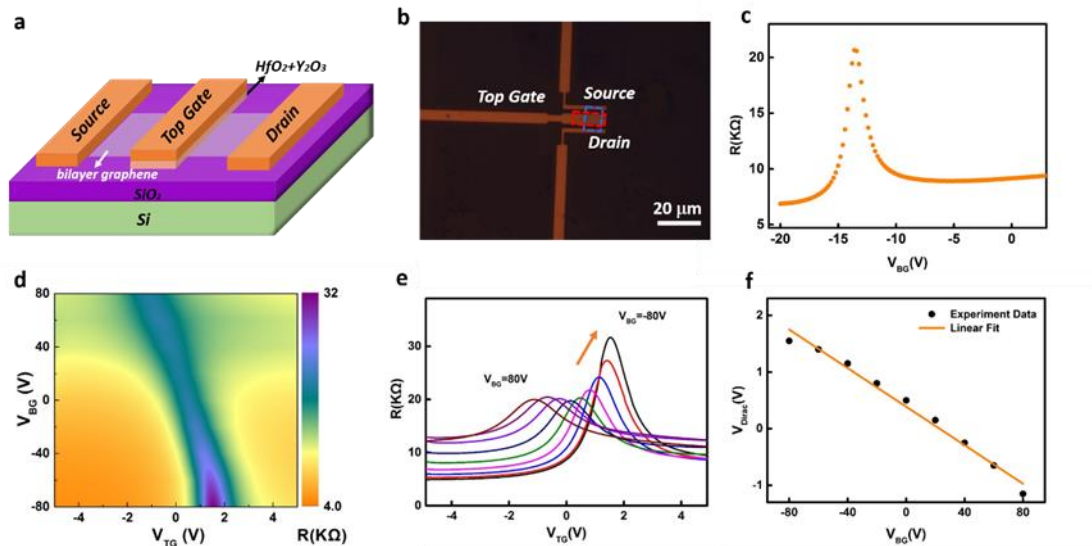


Figure 5. (a-b) Schematic structure diagram (a) and optical microscope image (b) of the BLG device with dual-gate applied for the transfer characteristics measurements. The BLG sheet and dielectric layer are marked by the blue and red dashed frame, respectively. (c) Plots of device resistance (R) versus back-gate voltage (V_{BG}). (d) Two-dimensional plot of resistance as functions of both top-gate voltage (V_{TG}) and V_{BG} of the dual-gate BLG device. (e) Resistance measured as a function of the top-gate voltage (V_{TG}) at a range of fixed back-gate voltages (V_{BG}) from -80 V to $+80$ V. The traces were taken at 20 V steps in the back-gate voltage. (f) Linear relation between the top-gate neutral points and the back-gate voltages.

To further evaluate the electronic quality of the BLG films, we fabricated the dual-gate graphene field-effect transistors (FETs). The schematic structure of the device is shown in Figure 5a (See Experimental Section for more details). As we know, Hafnium oxide (HfO_2) film couldn't be directly grown on graphene layers by atomic layer deposition (ALD)⁵⁹. Therefore, an ultrathin Yttrium oxide (Y_2O_3) film (5 nm) is grown on graphene film as the gate dielectric layer before depositing HfO_2 to provide ideal gate dielectric for graphene-based FETs⁶⁰⁻⁶¹. Figure 5b shows the representative optical image of a dual-gate BLG device. The resistance R versus the back-gated voltage (V_{BG}) (R - V_{BG}) plot in Figure 5c shows typical ambipolar characteristics expected for the graphene devices and the back-gate mobility is extracted to be $2297 \text{ cm}^2/\text{Vs}$ based on the fitting method reported previously⁶². Furthermore, we swept the voltage of top gate (V_{TG}) from -4 V to 4 V at different back gate voltages (V_{BG}) from -80 V to 80 V applied on the silicon substrate. The two-dimensional plot of the device resistance R versus V_{TG} and V_{BG} show that the highest resistance is achieved in the highest displacement field region (top middle left and bottom middle right) (Figure 5d). This can be more evidently illustrated in a series of plots of R - V_{TG} at different V_{BG} in Figure 5e, confirming the AB stacking nature of the bilayer graphene⁶³. For each trace, a resistance maximum, corresponding to the charge neutrality point (CNP), was seen. The CNP resistance is adjusted by tuning the vertical electric field which proves the formation of a tunable band structure^{12, 20, 58}. This was confirmed by the observation of an enhancement in the current on/off ratio. Figure 5e also shows that the $I_{\text{on}}/I_{\text{off}}$ values obtained in all measurements were about 1.66 and 6.46 for $V_{\text{BG}} = 80 \text{ V}$ and -80 V , respectively. Figure

5f shows that V_{Dirac} and V_{BG} are linearly related with a slope of about -0.017, agrees well with the expected value of $-\varepsilon_{\text{BG}} d_{\text{TGall}} / \varepsilon_{\text{TGall}} d_{\text{BG}} = -0.027$, where ε and d correspond to the dielectric constant and thickness of the top gate (Y_2O_3 : $d_1 = 5$ nm, $\varepsilon_1 = 12$; HfO_2 : $d_2 = 20$ nm, $\varepsilon_2 = 12$, $d_{\text{TGall}} = 25$ nm, $\varepsilon_{\text{TGall}} = 12$) and the bottom gate (SiO_2 : $d_{\text{BG}} = 300$ nm, $\varepsilon_{\text{BG}} = 3.9$). The carrier mobility of the top-gate BLG on SiO_2/Si substrates is $1708 \text{ cm}^2/\text{Vs}$, which is comparable to those of CVD grown bilayer graphene on metal substrates⁵⁸. These results clearly demonstrate that the bilayer graphene obtained by the direct epitaxial growth method on Si wafer is of high-quality, and the proposed strategy provides a rational route to synthesis high-quality AB-stacked bilayer graphene directly on the dielectric substrates.

4. Conclusions

In conclusion, we have proposed a new method to grow bilayer and multilayer graphene directly on various dielectric substrates. The quality and stacking order of bilayer graphene were confirmed by Raman spectroscopy, TEM diffraction patterns and dual gated FET measurements. Transport measurements show the bilayer AB-stacked graphene has a typical tunable transport band gap. The measured mobility of the bilayer graphene was $1708 \text{ cm}^2/\text{Vs}$, which is higher than other sample grown directly on insulating substrates. This Cu NP assisted graphene seeding growth technique can be beneficial for producing AB stacked bilayer graphene with high quality directly on insulating substrate, which is significant for the further development of functional graphene devices.

Acknowledgements:

We appreciate the support from the Beijing Natural Science Foundation through grant 2192024, the Fundamental Research Funds for the Central Universities and the Research Funds of Renmin University of China (Grant No. 21XNLG26).

Supplementary Material: Supplementary material is available in supporting information.

Reference

- (1) Geim, A. K.; Novoselov, K. S. The rise of graphene. *Nature Materials* **2007**, *6*, 183.
- (2) Bolotin, K. I.; Sikes, K.; Jiang, Z.; Klima, M.; Fudenberg, G.; Hone, J.; Kim, P.; Stormer, H. Ultrahigh electron mobility in suspended graphene. *Solid State Communications* **2008**, *146* (9-10), 351-355.
- (3) Dean, C. R.; Young, A. F.; Meric, I.; Lee, C.; Wang, L.; Sorgenfrei, S.; Watanabe, K.; Taniguchi, T.; Kim, P.; Shepard, K. L. Boron nitride substrates for high-quality graphene electronics. *Nature nanotechnology* **2010**, *5* (10), 722.
- (4) Li, X.; Cai, W.; An, J.; Kim, S.; Nah, J.; Yang, D.; Piner, R.; Velamakanni, A.; Jung, I.; Tutuc, E. Large-area synthesis of high-quality and uniform graphene films on copper foils. *science* **2009**, *324* (5932), 1312-1314.
- (5) Chen, S.; Ji, H.; Chou, H.; Li, Q.; Li, H.; Suk, J. W.; Piner, R.; Liao, L.; Cai, W.; Ruoff, R. S. Millimeter-size single-crystal graphene by suppressing evaporative loss of Cu during low pressure chemical vapor deposition. *Advanced Materials* **2013**, *25* (14), 2062-2065.
- (6) Zhao, P.; Kim, S.; Chen, X.; Einarsson, E.; Wang, M.; Song, Y.; Wang, H.; Chiashi, S.; Xiang, R.; Maruyama, S. Equilibrium chemical vapor deposition growth of Bernal-stacked bilayer graphene. *Acs Nano* **2014**, *8* (11), 11631-11638.
- (7) Hao, Y.; Bharathi, M.; Wang, L.; Liu, Y.; Chen, H.; Nie, S.; Wang, X.; Chou, H.; Tan, C.; Fallahzad, B. The role of surface oxygen in the growth of large single-crystal graphene on copper. *Science* **2013**, *342*(6159), 720-723.
- (8) Chae, S. J.; Güneş, F.; Kim, K. K.; Kim, E. S.; Han, G. H.; Kim, S. M.; Shin, H. J.; Yoon, S. M.; Choi, J. Y.; Park, M. H. Synthesis of large-area graphene layers on poly-nickel substrate by chemical vapor deposition: wrinkle formation. *Advanced Materials* **2009**, *21* (22), 2328-2333.
- (9) Gong, Y.; Zhang, X.; Liu, G.; Wu, L.; Geng, X.; Long, M.; Cao, X.; Guo, Y.; Li, W.; Xu, J. Layer-controlled and wafer-scale synthesis of uniform and high-quality graphene films on a polycrystalline nickel catalyst. *Advanced Functional Materials* **2012**, *22* (15), 3153-3159.
- (10) Yu, Q.; Lian, J.; Siriponglert, S.; Li, H.; Chen, Y. P.; Pei, S.-S. Graphene segregated on Ni surfaces and transferred to insulators. *Applied Physics Letters* **2008**, *93* (11), 113103.
- (11) Kim, K. S.; Zhao, Y.; Jang, H.; Lee, S. Y.; Kim, J. M.; Kim, K. S.; Ahn, J.-H.; Kim, P.; Choi, J.-Y.; Hong, B. H. Large-scale pattern growth of graphene films for stretchable transparent electrodes. *Nature*

2009, 457 (7230) ,706-710.

(12) Lee, S.; Lee, K.; Zhong, Z. Wafer Scale Homogeneous Bilayer Graphene Films by Chemical Vapor Deposition. *Nano Letters* **2010**, 10 (11), 4702-4707.

(13) Li, Q.; Chou, H.; Zhong, J.-H.; Liu, J.-Y.; Dolocan, A.; Zhang, J.; Zhou, Y.; Ruoff, R. S.; Chen, S.; Cai, W. Growth of Adlayer Graphene on Cu Studied by Carbon Isotope Labeling. *Nano Letters* **2013**, 13 (2), 486-490.

(14) Gulotty, R.; Das, S.; Liu, Y.; Sumant, A. V. Effect of hydrogen flow during cooling phase to achieve uniform and repeatable growth of bilayer graphene on copper foils over large area. *Carbon* **2014**, 77, 341-350.

(15) Chan, C.-C.; Chung, W.-L.; Woon, W.-Y. Nucleation and growth kinetics of multi-layered graphene on copper substrate. *Carbon* **2018**, 135, 118-124.

(16) Ning, Y.; Kyoungjun, C.; John, R.; Hyung Gyu, P. Layer-selective synthesis of bilayer graphene via chemical vapor deposition. *2D Materials* **2017**, 4 (3), 035023.

(17) Fang, W.; Hsu, A. L.; Song, Y.; Birdwell, A. G.; Amani, M.; Dubey, M.; Dresselhaus, M. S.; Palacios, T.; Kong, J. Asymmetric Growth of Bilayer Graphene on Copper Enclosures Using Low-Pressure Chemical Vapor Deposition. *ACS Nano* **2014**, 8 (6), 6491-6499.

(18) Hao, Y.; Wang, L.; Liu, Y.; Chen, H.; Wang, X.; Tan, C.; Nie, S.; Suk, J. W.; Jiang, T.; Liang, T.; Xiao, J.; Ye, W.; Dean, C. R.; Yakobson, B. I.; McCarty, K. F.; Kim, P.; Hone, J.; Colombo, L.; Ruoff, R. S. Oxygen-activated growth and bandgap tunability of large single-crystal bilayer graphene. *Nature Nanotechnology* **2016**, 11(5), 426-431.

(19) Yoo, M. S.; Lee, H. C.; Lee, S.; Lee, S. B.; Lee, N.-S.; Cho, K. Chemical Vapor Deposition of Bernal-Stacked Graphene on a Cu Surface by Breaking the Carbon Solubility Symmetry in Cu Foils. *Advanced Materials* **2017**, 29 (32), 1700753.

(20) Yan, K.; Peng, H.; Zhou, Y.; Li, H.; Liu, Z. Formation of Bilayer Bernal Graphene: Layer-by-Layer Epitaxy via Chemical Vapor Deposition. *Nano Letters* **2011**, 11 (3), 1106-1110.

(21) Park, J.; An, H.; Choi, D.-C.; Hussain, S.; Song, W.; An, K.-S.; Lee, W.-J.; Lee, N.; Lee, W.-G.; Jung, J. Selective growth of graphene in layer-by-layer via chemical vapor deposition. *Nanoscale* **2016**, 8 (30), 14633-14642.

(22) Liu, W.; Li, H.; Xu, C.; Khatami, Y.; Banerjee, K. Synthesis of high-quality monolayer and bilayer graphene on copper using chemical vapor deposition. *Carbon* **2011**, 49 (13), 4122-4130.

(23) Wu, J.; Wang, J.; Pan, D.; Li, Y.; Jiang, C.; Li, Y.; Jin, C.; Wang, K.; Song, F.; Wang, G.; Zhang, H.; Wan, J. Synchronous Growth of High-Quality Bilayer Bernal Graphene: From Hexagonal Single-Crystal Domains to Wafer-Scale Homogeneous Films. *Advanced Functional Materials* **2017**, 27 (22), 1605927.

(24) Han, J.; Lee, J.-Y.; Yeo, J.-S. Large-area layer-by-layer controlled and fully bernal stacked synthesis of graphene. *Carbon* **2016**, 105, 205-213.

(25) Takesaki, Y.; Kawahara, K.; Hibino, H.; Okada, S.; Tsuji, M.; Ago, H. Highly Uniform Bilayer Graphene on Epitaxial Cu–Ni(111) Alloy. *Chemistry of Materials* **2016**, 28 (13), 4583-4592.

(26) Chen, S.; Cai, W.; Piner, R. D.; Suk, J. W.; Wu, Y.; Ren, Y.; Kang, J.; Ruoff, R. S. Synthesis and characterization of large-area graphene and graphite films on commercial Cu–Ni alloy foils. *Nano letters* **2011**, 11 (9), 3519-3525.

(27) Liu, W.; Kraemer, S.; Sarkar, D.; Li, H.; Ajayan, P. M.; Banerjee, K. Controllable and Rapid Synthesis of High-Quality and Large-Area Bernal Stacked Bilayer Graphene Using Chemical Vapor Deposition. *Chemistry of Materials* **2014**, 26 (2), 907-915.

(28) Gao, Z.; Zhang, Q.; Naylor, C. H.; Kim, Y.; Abidi, I. H.; Ping, J.; Ducos, P.; Zauberman, J.; Zhao,

- M.-Q.; Rappe, A. M.; Luo, Z.; Ren, L.; Johnson, A. T. C. Crystalline Bilayer Graphene with Preferential Stacking from Ni–Cu Gradient Alloy. *ACS Nano* **2018**, 12 (3), 2275-2282.
- (29) Chen, J.; Guo, Y.; Jiang, L.; Xu, Z.; Huang, L.; Xue, Y.; Geng, D.; Wu, B.; Hu, W.; Yu, G.; Liu, Y. Near-Equilibrium Chemical Vapor Deposition of High-Quality Single-Crystal Graphene Directly on Various Dielectric Substrates. *Advanced Materials* **2013**, 26 (9), 1348-1353.
- (30) Chen, J.; Guo, Y.; Wen, Y.; Huang, L.; Xue, Y.; Geng, D.; Wu, B.; Luo, B.; Yu, G.; Liu, Y. Two-Stage Metal-Catalyst-Free Growth of High-Quality Polycrystalline Graphene Films on Silicon Nitride Substrates. *Advanced Materials* **2012**, 25 (7), 992-997.
- (31) Yan, Z.; Peng, Z.; Sun, Z.; Yao, J.; Zhu, Y.; Liu, Z.; Ajayan, P. M.; Tour, J. M. Growth of Bilayer Graphene on Insulating Substrates. *ACS Nano* **2011**, 5 (10), 8187-8192.
- (32) Sun, J.; Gao, T.; Song, X.; Zhao, Y.; Lin, Y.; Wang, H.; Ma, D.; Chen, Y.; Xiang, W.; Wang, J.; Zhang, Y.; Liu, Z. Direct Growth of High-Quality Graphene on High- κ Dielectric SrTiO₃ Substrates. *Journal of the American Chemical Society* **2014**, 136 (18), 6574-6577.
- (33) Murakami, K.; Tanaka, S.; Hirukawa, A.; Hiyama, T.; Kuwajima, T.; Kano, E.; Takeguchi, M.; Fujita, J.-i. Direct synthesis of large area graphene on insulating substrate by gallium vapor-assisted chemical vapor deposition. *Applied Physics Letters* **2015**, 106 (9), 093112.
- (34) Zhuo, Q.-Q.; Wang, Q.; Zhang, Y.-P.; Zhang, D.; Li, Q.-L.; Gao, C.-H.; Sun, Y.-Q.; Ding, L.; Sun, Q.-J.; Wang, S.-D.; Zhong, J.; Sun, X.-H.; Lee, S.-T. Transfer-Free Synthesis of Doped and Patterned Graphene Films. *ACS Nano* **2015**, 9 (1), 594-601.
- (35) Tan, L.; Zeng, M.; Wu, Q.; Chen, L.; Wang, J.; Zhang, T.; Eckert, J.; Rummeli, M. H.; Fu, L. Direct Growth of Ultrafast Transparent Single-Layer Graphene Defoggers. *Small* **2014**, 11 (15), 1840-1846.
- (36) Wei, D.; Lu, Y.; Han, C.; Niu, T.; Chen, W.; Wee, A. T. S. Critical Crystal Growth of Graphene on Dielectric Substrates at Low Temperature for Electronic Devices. *Angewandte Chemie* **2013**, 125 (52), 14371-14376.
- (37) Kim, H.; Song, I.; Park, C.; Son, M.; Hong, M.; Kim, Y.; Kim, J. S.; Shin, H.-J.; Baik, J.; Choi, H. C. Copper-Vapor-Assisted Chemical Vapor Deposition for High-Quality and Metal-Free Single-Layer Graphene on Amorphous SiO₂ Substrate. *ACS Nano* **2013**, 7 (8), 6575-6582.
- (38) Kwak, J.; Chu, J. H.; Choi, J.-K.; Park, S.-D.; Go, H.; Kim, S. Y.; Park, K.; Kim, S.-D.; Kim, Y.-W.; Yoon, E.; Kodambaka, S.; Kwon, S.-Y. Near room-temperature synthesis of transfer-free graphene films. *Nature Communications* **2012**, 3 (1), 1-7.
- (39) Su, C.-Y.; Lu, A.-Y.; Wu, C.-Y.; Li, Y.-T.; Liu, K.-K.; Zhang, W.; Lin, S.-Y.; Juang, Z.-Y.; Zhong, Y.-L.; Chen, F.-R.; Li, L.-J. Direct Formation of Wafer Scale Graphene Thin Layers on Insulating Substrates by Chemical Vapor Deposition. *Nano Letters* **2011**, 11 (9), 3612-3616.
- (40) Zhang, L.; Shi, Z.; Wang, Y.; Yang, R.; Shi, D.; Zhang, G. Catalyst-free growth of nanographene films on various substrates. *Nano Research* **2011**, 4 (3), 315-321.
- (41) Chen, J.; Wen, Y.; Guo, Y.; Wu, B.; Huang, L.; Xue, Y.; Geng, D.; Wang, D.; Yu, G.; Liu, Y. Oxygen-Aided Synthesis of Polycrystalline Graphene on Silicon Dioxide Substrates. *Journal of the American Chemical Society* **2011**, 133 (44), 17548-17551.
- (42) Baek, J.; Kim, J.; Kim, J.; Shin, B.; Jeon, S. Growth of graphene on non-catalytic substrate by controlling the vapor pressure of catalytic nickel. *Carbon* **2019**, 143, 294-299.
- (43) Nguyen, P.; Behura, S. K.; Seacrist, M. R.; Berry, V. Intergrain Diffusion of Carbon Radical for Wafer-Scale, Direct Growth of Graphene on Silicon-Based Dielectrics. *ACS Applied Materials & Interfaces* **2018**, 10 (31), 26517-26525.
- (44) Lee, E.; Lee, S. G.; Lee, H. C.; Jo, M.; Yoo, M. S.; Cho, K. Direct Growth of Highly Stable Patterned

Graphene on Dielectric Insulators using a Surface-Adhered Solid Carbon Source. *Advanced Materials* **2018**, 30 (15), 1706569.

(45) Hwang, J.; Kim, M.; Campbell, D.; Alsalman, H. A.; Kwak, J. Y.; Shivaraman, S.; Woll, A. R.; Singh, A. K.; Hennig, R. G.; Gorantla, S.; Rummeli, M. H.; Spencer, M. G. van der Waals Epitaxial Growth of Graphene on Sapphire by Chemical Vapor Deposition without a Metal Catalyst. *ACS Nano* **2013**, 7 (1), 385-395.

(46) Chen, X.-D.; Chen, Z.; Jiang, W.-S.; Zhang, C.; Sun, J.; Wang, H.; Xin, W.; Lin, L.; Priyadarshi, M. K.; Yang, H.; Liu, Z.-B.; Tian, J.-G.; Zhang, Y.; Zhang, Y.; Liu, Z. Fast Growth and Broad Applications of 25-Inch Uniform Graphene Glass. *Advanced Materials* **2017**, 29 (1), 1603428.

(47) Sun, J.; Chen, Y.; Priyadarshi, M. K.; Chen, Z.; Bachmatiuk, A.; Zou, Z.; Chen, Z.; Song, X.; Gao, Y.; Rummeli, M. H.; Zhang, Y.; Liu, Z. Direct Chemical Vapor Deposition-Derived Graphene Glasses Targeting Wide Ranged Applications. *Nano Letters* **2015**, 15 (9), 5846-5854.

(48) Chen, Y.; Sun, J.; Gao, J.; Du, F.; Han, Q.; Nie, Y.; Chen, Z.; Bachmatiuk, A.; Priyadarshi, M. K.; Ma, D.; Song, X.; Wu, X.; Xiong, C.; Rummeli, M. H.; Ding, F.; Zhang, Y.; Liu, Z. Growing Uniform Graphene Disks and Films on Molten Glass for Heating Devices and Cell Culture. *Advanced Materials* **2015**, 27 (47), 7839-7846.

(49) Tang, S.; Wang, H.; Wang, H. S.; Sun, Q.; Zhang, X.; Cong, C.; Xie, H.; Liu, X.; Zhou, X.; Huang, F.; Chen, X.; Yu, T.; Ding, F.; Xie, X.; Jiang, M. Silane-catalysed fast growth of large single-crystalline graphene on hexagonal boron nitride. *Nature Communications* **2015**, 6(1), 1-7.

(50) Yang, W.; Chen, G.; Shi, Z.; Liu, C.-C.; Zhang, L.; Xie, G.; Cheng, M.; Wang, D.; Yang, R.; Shi, D.; Watanabe, K.; Taniguchi, T.; Yao, Y.; Zhang, Y.; Zhang, G. Epitaxial growth of single-domain graphene on hexagonal boron nitride. *Nature Materials* **2013**, 12(9), 792-797.

(51) Shin, J. H.; Kim, S. H.; Kwon, S. S.; Park, W. I. Direct CVD growth of graphene on three-dimensionally-shaped dielectric substrates. *Carbon* **2018**, 129, 785-789.

(52) Gao, L.; Ren, W.; Xu, H.; Jin, L.; Wang, Z.; Ma, T.; Ma, L.-P.; Zhang, Z.; Fu, Q.; Peng, L.-M. Repeated growth and bubbling transfer of graphene with millimetre-size single-crystal grains using platinum. *Nature communications* **2012**, 3(1), 1-7.

(53) Liu, W.; Kraemer, S.; Sarkar, D.; Li, H.; Ajayan, P. M.; Banerjee, K. Controllable and rapid synthesis of high-quality and large-area Bernal stacked bilayer graphene using chemical vapor deposition. *Chemistry of Materials* **2013**, 26 (2), 907-915.

(54) Li, X.; Magnuson, C. W.; Venugopal, A.; Tromp, R. M.; Hannon, J. B.; Vogel, E. M.; Colombo, L.; Ruoff, R. S. Large-area graphene single crystals grown by low-pressure chemical vapor deposition of methane on copper. *Journal of the American Chemical Society* **2011**, 133 (9), 2816-2819.

(55) Ferrari, A. C.; Robertson, J. Interpretation of Raman spectra of disordered and amorphous carbon. *Physical Review B* **2000**, 61 (20), 14095-14107.

(56) Cançado, L. G.; Jorio, A.; Ferreira, E. H. M.; Stavale, F.; Achete, C. A.; Capaz, R. B.; Moutinho, M. V. O.; Lombardo, A.; Kulmala, T. S.; Ferrari, A. C. Quantifying Defects in Graphene via Raman Spectroscopy at Different Excitation Energies. *Nano Letters* **2011**, 11 (8), 3190-3196.

(57) Chen, J.; Guo, Y.; Jiang, L.; Xu, Z.; Huang, L.; Xue, Y.; Geng, D.; Wu, B.; Hu, W.; Yu, G. Near Equilibrium Chemical Vapor Deposition of High Quality Single Crystal Graphene Directly on Various Dielectric Substrates. *Advanced Materials* **2014**, 26 (9), 1348-1353.

(58) Liu, L.; Zhou, H.; Cheng, R.; Yu, W. J.; Liu, Y.; Chen, Y.; Shaw, J.; Zhong, X.; Huang, Y.; Duan, X. High-yield chemical vapor deposition growth of high-quality large-area AB-stacked bilayer graphene. *Acs Nano* **2012**, 6 (9), 8241-8249.

- (59) Lu, Y.; Bangsaruntip, S.; Wang, X.; Zhang, L.; Nishi, Y.; Dai, H. DNA functionalization of carbon nanotubes for ultrathin atomic layer deposition of high κ dielectrics for nanotube transistors with 60 mv/decade switching. *Journal of the American Chemical Society* **2006**, 128 (11), 3518-3519.
- (60) Xu, H.; Zhang, Z.; Xu, H.; Wang, Z.; Wang, S.; Peng, L.-M. Top-gated graphene field-effect transistors with high normalized transconductance and designable dirac point voltage. *ACS nano* **2011**, 5 (6), 5031-5037.
- (61) Wang, Z.; Xu, H.; Zhang, Z.; Wang, S.; Ding, L.; Zeng, Q.; Yang, L.; Pei, T.; Liang, X.; Gao, M. Growth and performance of yttrium oxide as an ideal high- κ gate dielectric for carbon-based electronics. *Nano letters* **2010**, 10 (6), 2024-2030.
- (62) Kim, S.; Nah, J.; Jo, I.; Shahrjerdi, D.; Colombo, L.; Yao, Z.; Tutuc, E.; Banerjee, S. K. Realization of a high mobility dual-gated graphene field-effect transistor with Al₂O₃ dielectric. *Applied Physics Letters* **2009**, 94 (6), 062107.
- (63) Yu, W. J.; Liao, L.; Chae, S. H.; Lee, Y. H.; Duan, X. Toward tunable band gap and tunable dirac point in bilayer graphene with molecular doping. *Nano letters* **2011**, 11 (11), 4759-4763.

Supplementary Material

1. First-principles DFT calculations

The adsorption energies of the first carbon atom adsorbed on multilayer graphene substrates (E_{ads}^{1st}) and the second atom adsorbed on multilayer graphene (E_{ads}^{2nd}) are defined as:

$$E_{ads}^{1st} = E_{total}^{one} - E_{multi} - E_{single},$$

and

$$E_{ads}^{2nd} = E_{total}^{two} - E_{total}^{one} - E_{single},$$

where E_{total}^{one} and E_{total}^{two} are total energies of one carbon atom and two carbon atoms adsorbed on multilayer graphene, respectively; E_{multi} is the energy of multilayers graphene, and E_{single} is the energy of single carbon atom.

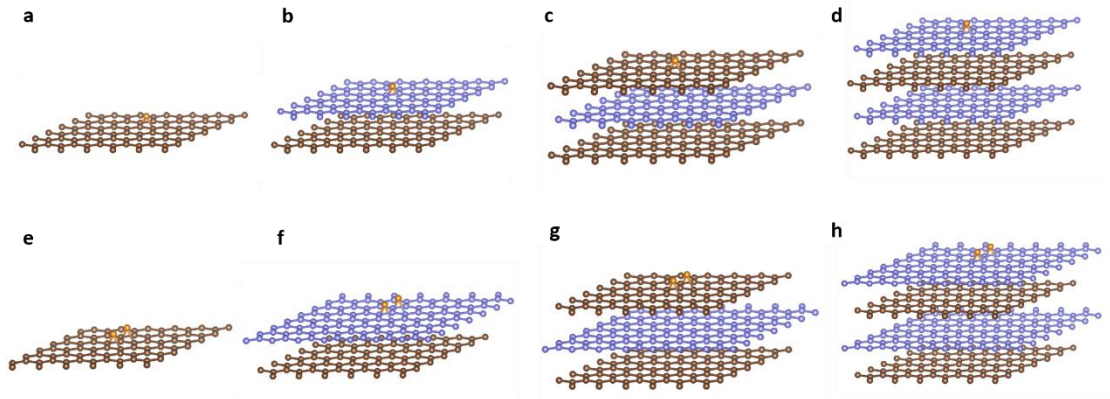


Figure S1. Atomic configurations of single carbon atom (a-d) and carbon dimer (e-h) adsorbed on monolayer and multilayer graphene.

2. BLG domains grown on quartz and sapphire

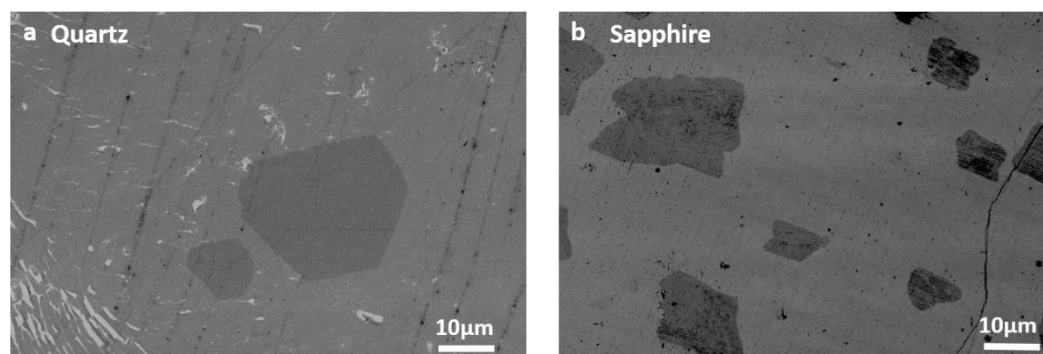


Figure S2. SEM images of the graphene grown on graphene seeding layers transferred onto quartz and sapphire substrates, respectively.